LEGIBILITY NOTICE

A major purpose of the Technical Information Center is to provide the broadest dissemination possible of information contained in DOE's Research and Development Reports to business, industry, the academic community, and federal, state and local governments.

Although a small portion of this report is not reproducible, it is being made available to expedite the availability of information on the research discussed herein.

1

LA-UR -90-99

CONF-9006476--1

Los Alamos National Laboratory is operated by the University of California for the United States Department of Energy under contract W-7405-ENG-36

LA-UR--90-99

DE90 006481

TITLE: Liquification of Fluid Saturated Rocks Due to Explosion-Induced Stress Waves

AUTHOR(S): T. Dey, and J. A. Brown

SUBMITTED TO: 31st U. S. Rock Mechanics Symposium, Colorado School of Mines, Golden, Colorado, June 18-20, 1990

Los Alamos

Los Alamos National Laboratory
Los Alamos, New Mexico 87545

Liquifaction of fluid saturated rocks due to explosion-induced stress waves

T. N. Dey and J. A. Brown
Earth and Environmental Sciences Division
Los Alamos National Laboratory
Los Alamos, NM 87545

ABSTRACT

Shock-induced liquifaction of a water-saturated rock may occur during the passage of a large amplitude stress wave, such as that due to an explosive. We studied this phenomena numerically with the aid of a material model which incorporates effective stress principles, and experimentally with a gas gun. Our numerical model is capable of calculating material response for both small and large deformation and any initial saturation. Phase transitions of the solid phase and the water phase are also allowed. Fitting the model to dry gas gun experiments allowed reasonable predictions of nearly saturated experiments. Liquifaction, the loss of shear strength when pore pressure exceeds the mean stress, appears to occur during the unloading portion of these experiments. The pore crushing which occurs, even under fully saturated conditions, leads to greater attenuation of a stress wave, as well as liquifaction of the rock and a lengthening of the wave duration, as the wave passes.

1. INTRODUCTION

The mechanical behavior of many water saturated rocks and soils is known to follow the law of effective stress. This means that a property, such as modulus or shear strength, is a function of $P_c - \alpha P_p$, where P_c is the mean total stress and Pp is the pore water pressure, and alpha may be a constant or depend on other conditions. Most modeling of deformation behavior has assumed infinitesimal strain conditions with the theory by Biot (1941), (Biot and Willis 1957) being one of the most important examples. More recently, Carroll (1980) and coworkers (Carroll and Holt 1972, Curran and Carroll 1979, Katsube and Carroll 1987a,b) have been important contributors to this field, with models useful for finite strain problems and materials with spherical pores. Models useful for large amplitude wave propagation studies are fewer in number. The large amplitude problem adds to the complexities of non-linear response of the pore water and the rock solids, as well as pore crushing, shear and tensile failure. The model by Swift and Burton (1984) is an example and uses an incremental approach to solve for the stresses at each computational cycle. Garg, et al (1974, 1975) also developed a numerical model for large amplitude problems and studied some 1-D wave propagation problems.

Fitting model parameters can be tedious and difficult, and the presence of phase transitions in the solids component of a rock adds a further level of complexity. Our model implementation reduces these difficulties and is well suited for use in finite difference stress wave propagation codes. After outlining the model, some examples of its use in stress wave propagation are shown. We also present results of gas gun experiments on dry and saturated limestone which demonstrate some of the results of the model.

2. NUMERICAL MODEL FOR EFFECTIVE STRESS RESPONSE

In contrast to most other effective stress models, which are formulated according to an incremental approach, this model uses the integrated quantities. In typical finite difference stress wave propagation codes, the specific volume is the known quantity at the start of each time step, and the new values of the stress tensor must be determined. For the P-V behavior of an effective stress material, the mean total stress, the pore water volume and the pore water pressure all must be found from this specific volume. We assume here that flow of water through the rock is small during the passage of a stress wave, ie. undrained conditions. To do this the following equations are defined:

(1) $$V_b(P, P_p, E) = V_p(P, P_p, E_w) + V_s(P, P_p, E_s)$$

(2) $$V_p(P, P_p, E_w) = \phi(P_{eff}) V_b(P, P_p, E) \quad .$$

We also use equation of state relationships for the solids and the water:

(3) $$V_s(P, P_p, E_s) = V_s(P_s, E_s),$$

and

(4) $$P_p = P_p(V_p, E_w) = P_w(V_w, E_w) \text{ for saturated conditions}$$

or

(5) $$P_p = 0 \text{ for unsaturated conditions} \quad .$$

The mean solids pressure and the effective pressure are defined as:

$$P_s = \frac{P_{eff}}{(1-\phi)} + P_p \tag{6}$$

$$P_{eff} = P - P_p \quad . \tag{7}$$

The remaining terms have the following definitions:

V_b: specific volume of the bulk material
V_p: pore volume
V_s: solids volume
V_w: pore water volume, $= V_p$ for saturated conditions
P: mean total stress
P_p: pore water pressure
P_s: mean stress in solids component
ϕ: porosity
E: specific internal energy of bulk material
E_s: specific internal energy of rock solids
E_w: specific internal energy of pore water

$V_s(P_s, E_s)$ and $P_w(V_w, E_w)$ are both found from equation of state tables. The porosity is assumed to be a function of only the effective pressure $P - P_p$, an assumption made by Carroll (1980) in his model development. Nur and Byerlee (1971) proved this assumption for materials with a linear elastic homogeneous solid phase. This same assumption is also implied by Equation 64 of Swift and Burton (1984). As pointed out by Carroll, this assumption has the advantage of allowing the solids response to be separated from the other contributions to the material response. In our implementation, the porosity-effective pressure relationship is used in tabular form and is generated directly from pressure-bulk volume measurements from drained experiments (P_p=0) by solving the relation

$$(1-\phi)V(P) = V_s\left(\frac{P}{(1-\phi)}\right) \tag{8}$$

assuming the solids $P - V$ relationship is known and where the substitution of equation (6) for the solids pressure has already been made. For a linear solid, equation (8) reduces to quadratic function of $(1-\phi)$ and is easily solved.

During a numerical simulation, equations (1)-(7) are solved simultaneously for P, P_p, and V_p. Note that all the parameters required to define the model, namely the equations of state of the solids and the water, as well as the porosity can be defined directly from experimental data.

Deviatoric response in the model is controlled by a shear failure envelope together with a shear modulus defined either directly or from a Poisson's ratio together with the current bulk modulus defined by the $P - V$ behavior.

The shear failure strength is assumed to depend on the effective pressure as defined by (7), which is the conventional assumption. Initial and ultimate failure envelopes are specified by tables which can be defined directly from triaxial strength tests. Interpolation between these two envelopes is done according to a hardening parameter based on the plastic work. Dilatancy and shear-enhanced void collapse are incorporated by either an associated or general non-associated flow rule, which then feeds back to the $P-V$ behavior by a porosity adjustment. Curran and Carroll (1979) were able to treat shear-enhanced void collapse with their spherical pore model. In general, both this effect and dilatancy may occur in the same rock sample at different times in the same experiment, so we choose to leave this part of the model in a form which can be empirically fit to experimental data.

3. GAS GUN EXPERIMENTS

In order to better understand effective stress phenomena under dynamic loading conditions, we carried out a series of gas gun experiments on Lueder's limestone. This limestone has a porosity of about 16.5%, and samples were either dry or were saturated to between 90% and 100% of complete saturation. The samples, each about 20 cm diameter and 9 cm long, were impacted with either an aluminum or steel projectile through a 1.27 cm thick aluminum buffer plate. Projectile velocities of 150-175 m/s were chosen to give peak stress of 500-1000 MPa in the samples. The higher stresses are reached with saturated samples and with the steel projectiles. The samples were made of a sandwich of four rock disks so that carbon piezoresistive stress gages could be inserted in the interior of the sample at various ranges. The data from these gages are analyzed by Lagrangian analysis method (Seaman 1974) to give particle velocity, wave velocity and stress-strain curves.

Figures 1a-b show stress waveforms and longitudinal stress-longitudinal strain curves for a dry Lueders limestone sample. As should be expected, the stress wave in this sample is highly dispersive and shows a rapidly increasing rise time for gages located farther down the sample due to the dissipation from pore crushing which delays the remainder of the wave after the elastic precursor. The shoulder in the leading edge of the wave at 150-200 MPa on the stress-strain curves is due to the beginning of shear failure in the sample.

Figures 2a-b show similar plots for a sample which is approximately 92% saturated. Because the presence of water in the pores inhibits pore crushing, little dispersion or peak stress attenuation appears during the duration of the experiment. The slopes of the unloading stress-strain curves decrease by a factor of two as the stress drops. We believe the "glitch" in these curves at about 250 MPa is due to liquifaction of the sample. This is discussed further below.

4. DISCUSSION

Before continuing the discussion of the gas gun experiments, we show the following numerical wave propagation example to clarify a number of effective stress concepts and how they manifest themselves in a propagating wave. The laboratory data for shear strength and pressure-volume behavior used to set up this calculation are from unpublished data on Salem, Indiana limestone by S. Blouin of Applied Research Associates and J. Zelasko of the US Army Waterways Experiment Station.

Figure 3 shows the $P-V$ relationships for the limestone during a load-unload cycle. The peak mean stress in this cycle reaches about 575 MPa, while the compression of the pore space and the pore water in it generates a pore water pressure of about 425 MPa. The effective pressure, defined for this model as the difference between these two pressures, reaches a peak level of about 130 MPa. Even though this is a fully saturated material, this is still sufficient to cause partially irreversible pore crushing. This pore crushing then leads to the steeper unloading response for the material as a whole, and the hysteresis in the total $P-V$ curve. On unloading, the total pressure and the pore pressure curves intersect at about 220 MPa. At this point the effective pressure is zero and liquifaction is assumed to occur. At liquifaction, the model assumes that a condition of pervasive micro-hydraulic fracturing will occur, and consequently, further unloading will proceed with pressure equilibrium between the rock solids and the pore water. For materials with non-zero shear strength, the model assumes that this liquifaction condition will lead to total loss of shear strength.

An illustration of the use of this model in a wave propagation calculation is shown in Fig. 4. This calculation assumes 1-D uniaxial strain boundary conditions with a sawtooth wave of 10 ms duration applied as a pressure boundary condition. A sawtooth is a convenient simplification of the wave shape produced by an explosion. The waveforms in the figure are time-histories at 20 m intervals beginning at 20 m range. Near the end of each waveform, the point at which the liquifaction condition is reached is shown. The relatively shallow slope of the $P-V$ material response under these conditions (see Fig. 3) gives this portion of the wave a slower propagation speed and causes the tail of the wave to be stretched out as it propagates. The leading edge of the wave shows a break at about 150 MPa which is due to the softening of the $P-V$ response at this pressure caused by the onset of significant amounts of pore crushing. A more substantial break occurs at about 200 MPa and is due to the onset of shear failure.

These results put us in a position to understand the nearly saturated limestone experiment. We first modeled the dry experiment in a 1-D numerical model of the experimental apparatus. The effective pressure porosity table was adjusted until a reasonable fit of the dry limestone waveforms was obtained. We then used this to model the nearly saturated limestone experiment. Our results are shown in Figure 2b together with the experimental data. Only one of the numerical experiment's gage results is shown because they are so similar due to the negligible attentuation of the wave. The dashed line shows the numerical results for the total and effective longitudinal stress plotted against the longitudinal strain. The differences between the model results and the experiment are consistent with sample to sample variability we have observed in this limestone. Notice that between 25 and 30 millistrain during unloading the effective stress drops to zero leading to a liquifaction condition. This coincides with the "glitch" in the experimental stress-strain records and suggests the interpretation that liquifaction is also occuring in the gas gun experiment.

The carbon piezoresistive stress gages are contained within a thin (0.1 mm) layer of epoxy used to bond the rock disks together. Although this does not affect the stress wave risetime or the fidelity of the recorded peak stress, the abrupt change in shear stress across this boundary as the rock, but not the epoxy, liquifies can cause a change in gage response due to the slight transverse sensitivity of the gage element. The liquifaction of the rock can also allow a bending or buckling response of the thin epoxy layer. These effects have not been quantified. They would be best addressed experimentally because of the difficulty of numerically modeling the response of such a small inclusion. However, our qualitative interpretation is supported by the presence of the effect in all three gage records.

5. CONCLUSIONS

We have implemented a numerical model for effective stress phenomena and compared it to experimental results on nearly saturated limestone samples. We see good agreement between the model and the experimental data. The model indicates increased stress wave attenuation due to pore crushing under saturated conditions. This pore crushing also can lead to liquifaction of the rock after the peak of the stress wave passes. Such conditions should also occur near explosions in saturated rock masses.

6. ACKNOWLEDGEMENTS

This work was performed under the auspices of the U.S. Department of Energy.

7. REFERENCES

Biot, M.A. 1941. General theory of three dimensional consolidation. J. Appl. Phys. 12:155-165.

Biot, M.A., and D.G. Willis. 1957. The elastic coefficients of the theory of consolidation. J. Appl. Mech., 24:594-601.

Carroll, M.M.. 1980. Mechanical response of fluid-saturated porous materials. Proc. 15th International Congress on Theoretical and Applied Mechanics, F.P.J. Rimrott and R. Tabarrok eds., North Holland, NY, pp 251-262.

Carroll, M.M., and A.C. Holt. 1972. Static and dynamic pore-collapse relations for ductile porous materials. J. Appl. Mech. 43:1626-1636.

Curran, J.H., and M.M. Carroll. 1979. Shear stress enhancement of void compaction. J. Geophys. Res. 84:1105-1112.

Garg, S.K., A.H. Nayfeh, and A.J. Good. 1974. Compressional waves in fluid-saturated elastic porous media. J. Appl. Phys. 45:1968-1974.

Garg, S.K., D.H. Brownell, J.W. Pritchett, and R.G. Herrmann. 1975. Shock wave propagation in fluid-saturated porous media. J. Appl. Phys. 46:702-713.

Katsube, N., and M.M. Carroll. 1987. The modified mixture theory for fluid-filled porous materials: Theory. J. Appl. Mech. 54:35-40.

Katsube, N., and M.M. Carroll. 1987. The modified mixture theory for fluid-filled porous materials: Applications. J. Appl. Mech. 54:41-46.

Nur, A., and J.D. Byerlee. 1971. An exact effective stress law for elastic deformation of rock with fluids. J. Geophys. Res. 76:6414-6419.

Seaman, L. 1974. Lagrangian analysis for multiple stress or velocity gages in attenuating waves. J. Appl. Phys. 45:4304-4314.

Swift, R.P., and D.E. Burton. 1984. Numerical modeling of the mechanics of nonlinear porous media under dynamic loading. Lawrence Livermore Natl. Lab. Rept. UCRL-53568.

Figure Captions

Fig. 1. Stress-time histories from carbon gages embedded in a dry Lueders limestone sample at 1.273, 2.560, and 3.833 cm. The sample was loaded through a 1.278 cm thick aluminum plate by a 5.085 cm thick 1100-0 aluminum flyer impacting at 174.9 m/s. Stress-strain curves are derived by Lagrangian analysis.

Fig. 2. Stress-time histories for a 92.5% saturated Lueders limestone sample. Gages were located 1.295, 2.576, and 3.856 cm into the sample. Sample was loaded through a 1.270 cm thick aluminum plate by a 5.083 cm thick 6061-T6 aluminum flyer plate impacting at 170 m/s. Stress-strain curves are derived by Lagrangian analysis. Also shown by dashed lines are numerical model predictions.

Fig. 3. Uniaxial strain load-unload curves for a completely saturated limestone. Shown are the longitudinal stress component, the mean stress, the pore water pressure, and the effective mean stress, which is defined here as the difference between the mean total stress and the pore water pressure. Arrows indicate the loading portion of each curve.

Fig. 4. Time-histories of longitudinal stress for a sawtooth wave traveling under uniaxial strain conditions. Successive waveforms are at 20 m intervals along the direction of propagation.

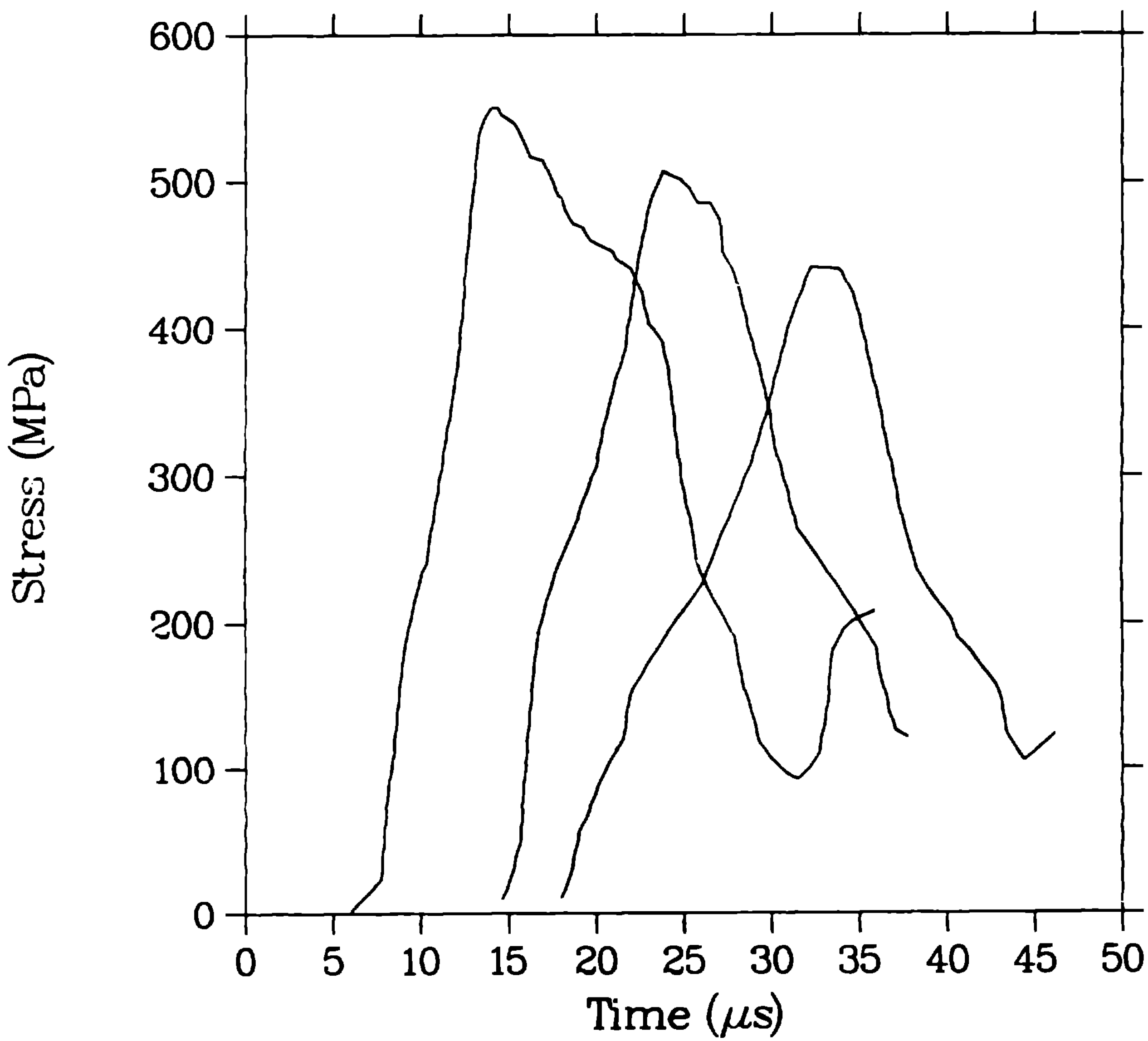

Stress (MPa)
600
500
400
300
200
100
0
0
5
10
15
20
25
30
35
40
45
50
Time (μs)

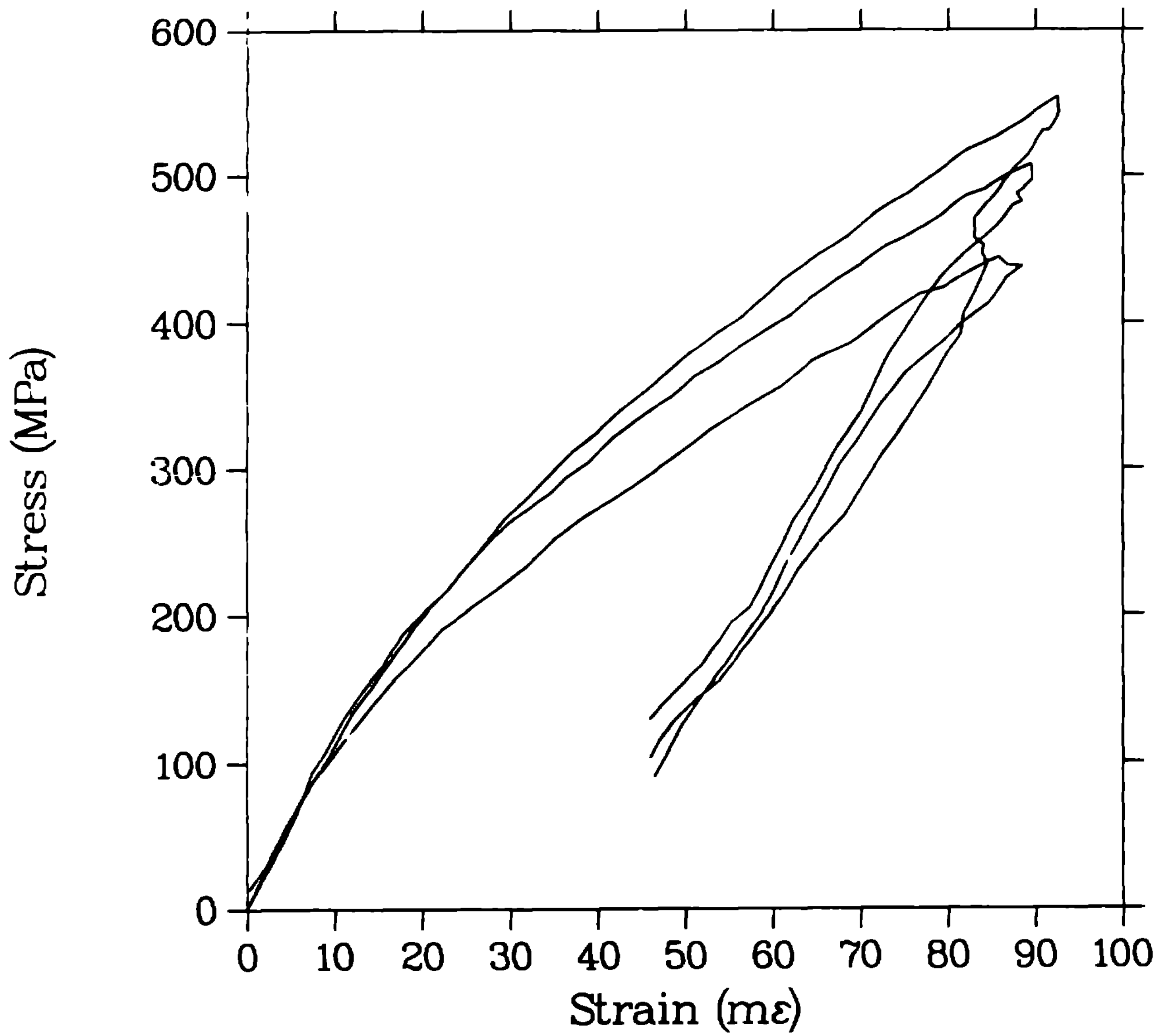

600
500
400
300
200
100
0
Stress (MPa)
0
10
20
30
40
50
60
70
80
90
100
Strain (mε)

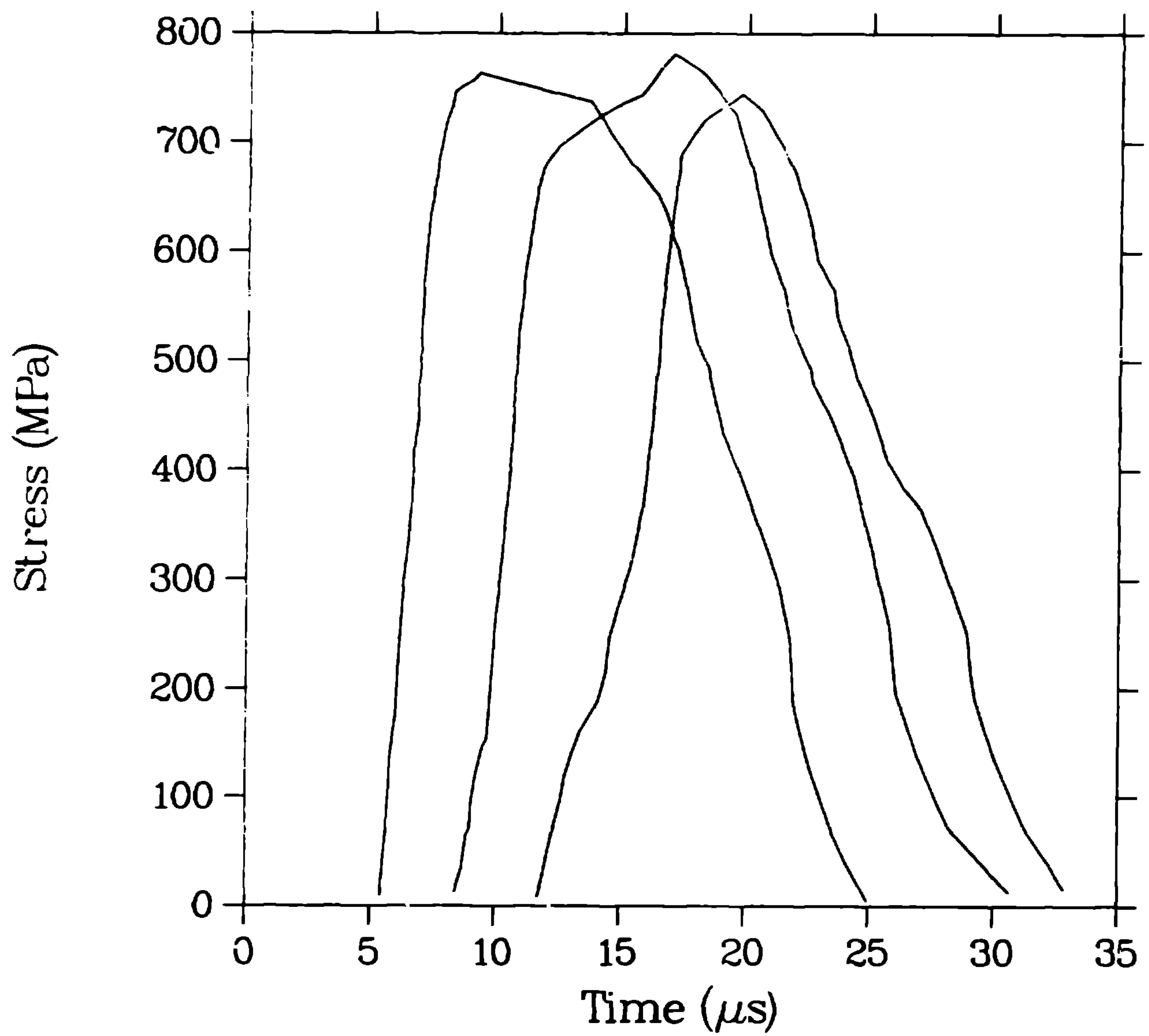

Stress (MPa)
800
700
600
500
400
300
200
100
0
0
5
10
15
20
25
30
35
Time (μs)

2b

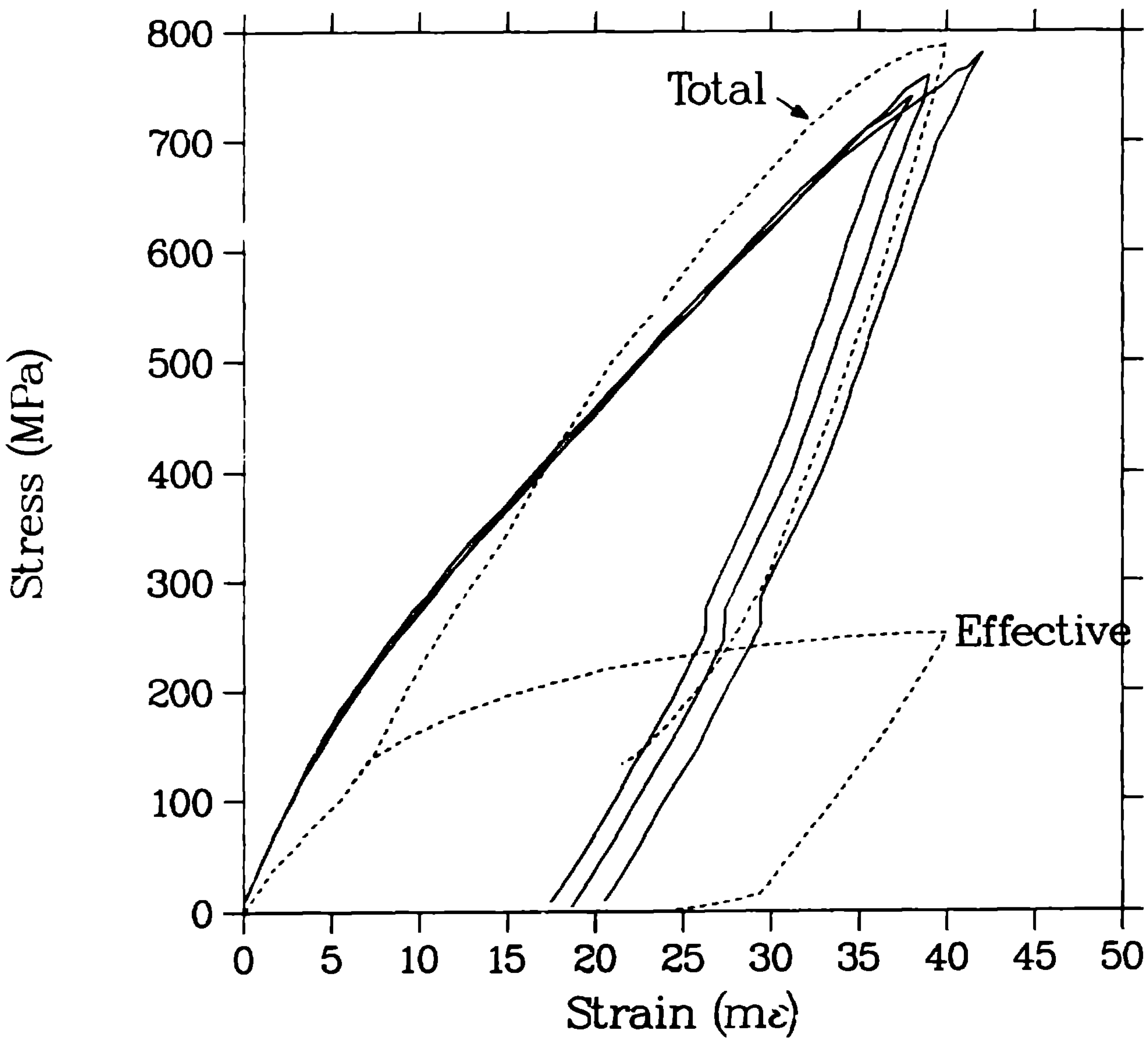
Stress (MPa)
800
700
600
500
400
300
200
100
0
Total
Effective
0
5
10
15
20
25
30
35
40
45
50
Strain (mε)

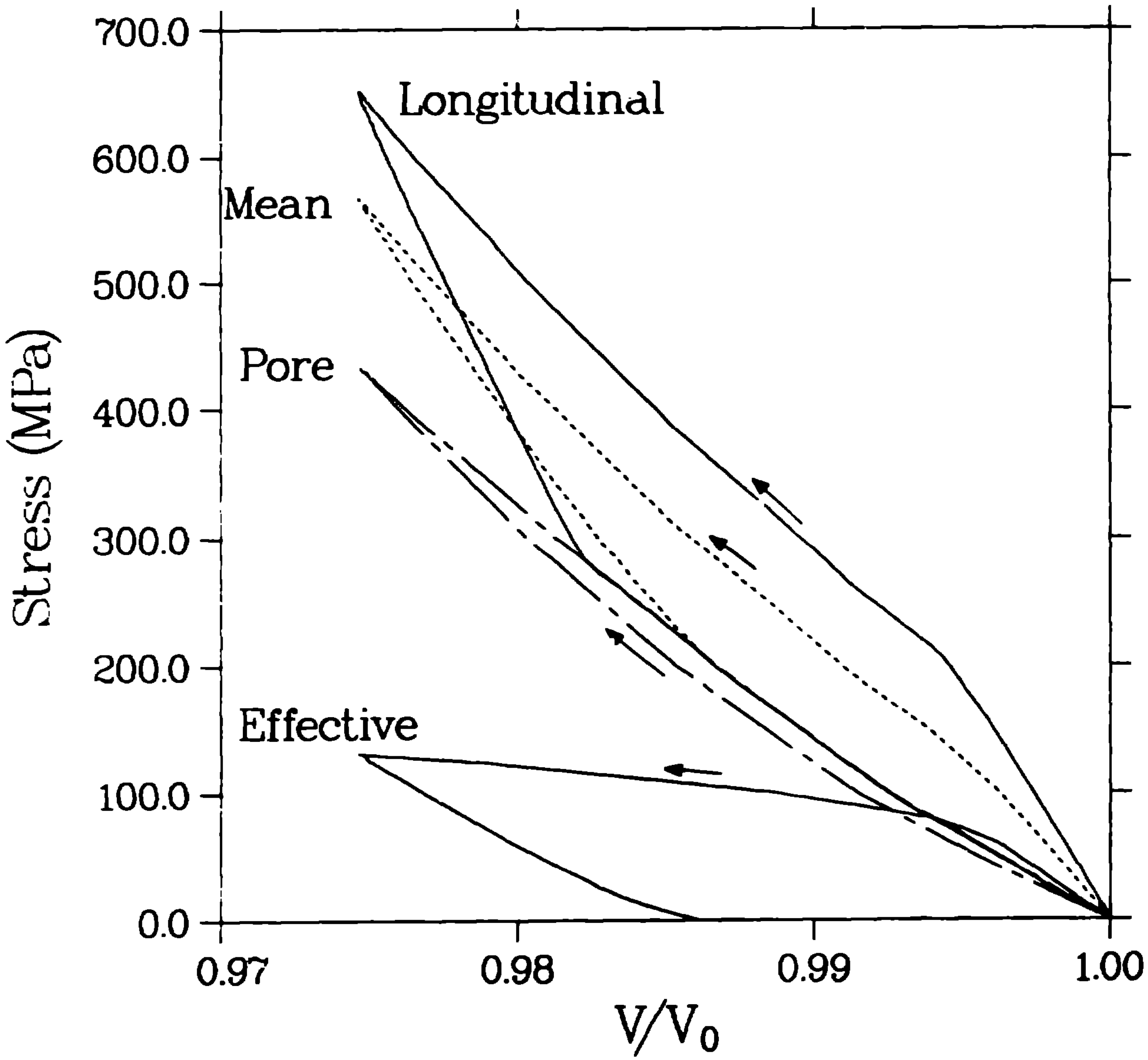

700.0
600.0
500.0
400.0
300.0
200.0
100.0
0.0
Stress (MPa)
Longitudinal
Mean
Pore
Effective
0.97
0.98
0.99
1.00
V/V0

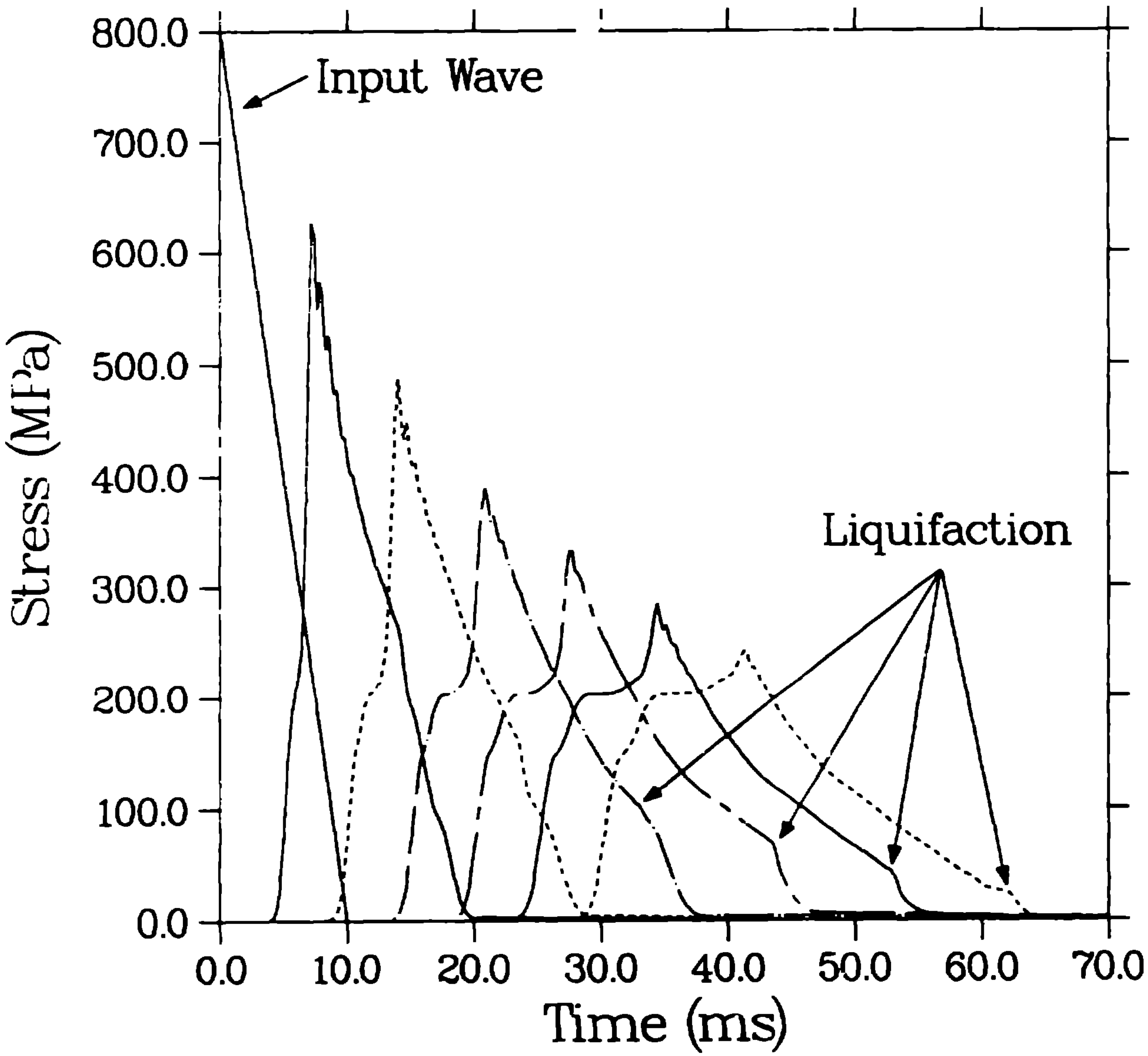

Input Wave
Liquifaction
Stress (MPa)
Time (ms)
800.0
700.0
600.0
500.0
400.0
300.0
200.0
100.0
0.0
0.0
10.0
20.0
30.0
40.0
50.0
60.0
70.0